PCCP

ROYAL SOCIETY OF CHEMISTRY

PAPER

View Article Online
View Journal | View Issue

Cite this: *Phys. Chem. Chem. Phys.*, 2024, **26**, 29449

The molecular mechanism of the triplet state formation in bodipy-phenoxazine photosensitizer dyads confirmed by *ab initio* prediction of the spin polarization†

Maria Kosaka, *[a] Katsuki Miyokawa [a] and Yuki Kurashige *[abc]

Efficient formation of excited triplet states on metal-free photosensitizer dyads, bodipy-phenoxazine (BDP-PXZ) and tetramethylbodipy-phenoxazine (TMBDP-PXZ), was investigated using *ab initio* calculations. We revealed the reason why two different triplet transient species, ^{3}CT and ^{3}BDP, can co-exist only for BDP-PXZ as observed in the previous study with the TR-EPR measurements. It was found that the state mixing of ^{3}CT enables the transition from ^{1}CT to ^{3}CT and ^{3}BDP states only for BDP-PXZ. This mixing effect is commonly seen in the singlet states of twisted intermolecular charge transfer molecules, though the key factor that determines the mixing of the excited states of the dyes was found to be the electron-donating ability of the substituents rather than their steric hindrance. This mechanism was corroborated by comparing the spin polarization ratio of the triplet spin-sublevels measured by TR-EPR with the theoretical predictions. The spin polarization ratio of the triplets should contain information about the transition *via* intersystem crossing, *e.g.* the twisted angle of two chromophores of the dyad, and thus it can be a powerful tool to analyze the molecular mechanism of photochemical processes at the electronic structure level. These insights on the molecular structures' effect provided by this theoretical study would be a compass to molecular design of metal-free triplet photosensitizers.

Received 29th August 2024,
Accepted 29th October 2024

DOI: 10.1039/d4cp03386h

rsc.li/pccp

1 Introduction

Triplet excited states of organic chromophores are some of the most familiar paramagnetic species in chemistry. Because their radiative and non-radiative decays to the ground state are spin-forbidden processes, they usually have a long enough lifetime to collide with or transfer the energy to other molecules, which allows for a wide range of applications, *e.g.*, photon upconversion,[1–5] triplet sensitizers,[6–10] dynamic nuclear polarization,[11–14] *etc.* Conversely, the generation of triplet excited states of metal-free organic chromophores by photo-irradiation is not so efficient because the spin–orbit coupling (SOC) which induces intersystem crossing (ISC) from the S_1 state to the T_n state is usually small, except for a few cases. One such exception is the transition between n–π* and π–π* excited states, in which the transition between the in-plane and out-of-plane 2p orbitals on an atom generates angular momentum, but there is a limited variety of organic chromophores with low-lying n–π* excited states.

The spin–orbit coupling induced by charge transfer (SOCT)[15,16] in covalently linked aromatic molecules is a promising alternative mechanism that can generate triplet states of a wide range of chromophores. For example, unsubstituted boron-dipyrromethene (BDP) and its derivatives have attracted attention for their unique properties.[17,18] They have high fluorescence quantum yields often approaching one, and thus it is difficult to obtain a sufficient quantity of triplets by photo-irradiation. Filatov and co-workers have successfully obtained the triplet excited state of BDP in their pioneering work using the SOCT-ISC mechanism.[19] A necessary condition for the SOCT should be that the energy levels of the singlet and triplet charge transfer states, *i.e.* ^{1}CT and ^{3}CT, lie between those of the singlet and triplet local excited states, ^{1}BDP and ^{3}BDP in this paper, and thus it should be valuable if we can predict energy levels of the excited states along the decay process using theoretical calculations.

To predict photochemical processes on covalently linked donor–accepter systems is still challenging because the characters of low-lying excited states drastically vary with the twist angle between the molecules, though they are hardly measurable with only a few exceptions[20] despite their importance.

[a] *Department of Chemistry, Graduate School of Science, Kyoto University, Kitashirakawa Oiwake-cho, Sakyo-ku Kyoto 606-8502, Japan. E-mail: kosaka@theoc.kuchem.kyoto-u.ac.jp, kura@kuchem.kyoto-u.ac.jp*
[b] *FOREST, JST, Honcho 4-1-8, Kawaguchi, Saitama 332-0012, Japan*
[c] *CREST, JST, Honcho 4-1-8, Kawaguchi, Saitama 332-0012, Japan*

† Electronic supplementary information (ESI) available. See DOI: https://doi.org/10.1039/d4cp03386h

The locally excited (LE) state responsible for the absorption/emission of photons is stabilized in the planar conformation, whereas the charge transfer (CT) state, which is sensitive to the polarity of the environment, is stabilized in the perpendicular conformation, and what complicates the situation is that these states can be mixed at the angle where they are close in energy. At the same time, it can be a strength if its character is well-designed. The sensitivity of the luminescence properties of the twisted intramolecular charge transfer (TICT) state is used for sensing environmental polarity, microenvironmental viscosity, and chemical species.[21,22] For highly efficient thermally activated delayed fluorescence materials (TADFs) for organic light-emitting diodes (OLEDs), the CT character can make the S_1–T_1 gap small, which enhances the reverse ISC, and the LE character will compensate for the lack of fluorescence efficiency.[23–26] For SOCT-ISC molecules, the subject of this study, the twist angle should also alter the SOC between the singlet and triplet excited states; thus, a detailed theoretical analysis based on the molecular structure is necessary.

Here, molecular mechanisms of the triplet state formation in the bodipy-phenoxazine (BDP-PXZ) dyads were investigated using quantum chemical calculations. Interestingly, it has been suggested that a small modification, an addition of the methyl groups, of the BDP moiety prevents the generation of the ^{3}CT state, while it was generated together with the ^{3}BDP state when the substituents were absent.[27] It was also suggested that ^{3}CT and ^{3}BDP states exhibit different EPR patterns, *i.e.*, different spin polarizations, which should contain the information of the spin-selective ISC that the molecules went through,[28] *e.g.* the twisted angle between the chromophores, and they can be used for the corroboration of the proposed mechanism by comparing with the theoretical predictions. However, the calculation method has not been established to predict the spin polarization in the magnetic axis for triplet states of organic chromophores, because quantitative calculations of the zero-field splitting (ZFS) *D*-tensor are necessary. Our recent developments in the prediction of the spin–spin coupling (SSC)[29] based on the *ab initio* density-matrix renormalization group (DMRG) algorithm opened up the possibility of quantitative prediction of the magnetic properties of organic chromophores. By comparing the theoretical predictions with the TR-EPR experimental results, we can confirm the character of the transient species and the mechanism at the electronic structure level.

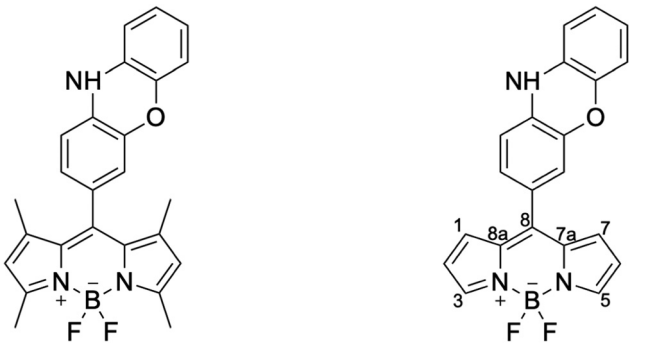

(a) TMBDP-PXZ (b) BDP-PXZ

Fig. 1 Chemical structures of BDP-PXZ and TMBDP-PXZ.

2 Computational details

Bodipy-phenoxazine dyads shown in Fig. 1 are adopted in this study, and the dyads synthesized experimentally are modeled by replacing the C_4H_9 alkyl-chain with a hydrogen atom.[27] Geometry optimizations were performed with the def2-TZVP basis sets[30–32] and a long-range corrected BLYP functional[33] (LC-BLYP) in which the range separation parameter was tuned to μ = 0.15 was adopted (see the ESI†). The polarizable continuum model[34] (PCM) was used to account for the solvent effect of toluene. All the excited states including the lowest triplet state were calculated by the time-dependent density functional theory (TD-DFT) using the ORCA5 program package.[35]

The matrix elements of spin–orbit coupling between the ^{1}CT and each spin sublevel (x, y, z axes of the molecular frame) of ^{3}CT and ^{3}BDP states were calculated by TD-DFT. The ZFS *D*-tensor was calculated using the method reported in ref. 29, in which the expected values of the spin–spin coupling operator in the Breit–Pauli Hamiltonian

$$\hat{H}_{\mathrm{SSC}} = \frac{g_e^2 \mu_B^2 \alpha^2}{2} \sum_{i \neq j} \left[\frac{\hat{\boldsymbol{s}}(i) \cdot \hat{\boldsymbol{s}}(j)}{r_{ij}^3} - \frac{3\left(\hat{\boldsymbol{s}}(i) \cdot \boldsymbol{r}_{ij}\right)\left(\hat{\boldsymbol{s}}(j) \cdot \boldsymbol{r}_{ij}\right)}{r_{ij}^5} \right], \quad (1)$$

where g_e is the electron *g*-factor, μ_B is the Bohr magneton, α is the fine structure constant, $\hat{\boldsymbol{s}}(i)$ is the spin operator of an electron i and $\boldsymbol{r}_{ij}$ is the distance between electrons i and j, were calculated by the contraction of the spin–spin coupling integrals d^{kl}_{pqrs} and the spin-dependent two-particle density matrices q_{pqrs} (2-RDM) as

$$D^{\mathrm{SSC}}_{kl} = \frac{g_e^2 \alpha^2}{4S(2S-1)} \sum_{pqrs} d^{kl}_{pqrs} q_{pqrs}, \quad (2)$$

where

$$d^{kl}_{pqrs} = \iint \phi_p(\boldsymbol{r}_1)\phi_r(\boldsymbol{r}_2) \frac{r_{12}^2 \delta_{kl} - 3(\boldsymbol{r}_{12})_k (\boldsymbol{r}_{12})_l}{r_{12}^5} \phi_q(\boldsymbol{r}_1)\phi_s(\boldsymbol{r}_2) \mathrm{d}\boldsymbol{r}_1 \mathrm{d}\boldsymbol{r}_2, \quad (3)$$

$$q_{pqrs} = \frac{1}{4}\langle \Psi | E_{pq}\delta_{sr} - S^z_{ps} S^z_{rq} + \frac{1}{2}\left(S^z_{pq} S^z_{rs} - E_{pq} E_{rs} \right) | \Psi \rangle. \quad (4)$$

The density matrix renormalization group self-consistent field (DMRG-SCF) theory[36–38] was used as a reference wavefunction of the spin-dependent 2-RDM. The spin–spin coupling integrals were efficiently calculated with the resolution of the identity (RI) approximation[39] implemented in the modified version of the PySCF library.[40] Once the *D*-tensor was calculated, the 3 × 3 tensor was diagonalized to obtain the energy gaps of the spin-sublevels that correspond to the *D* and *E* values with the sign convention of ESR experiment.

3 Results

3.1 Molecular mechanism of the formation of the triplet states

To elucidate the molecular mechanism of the formation of the triplet states, we performed the geometry optimization for ^{1}CT, ^{3}CT, and ^{3}BDP states with constraints for the dihedral angle θ between BDP and PXZ moieties. Fig. 2 shows the potential energy curves (PECs) of TMBDP-PXZ and BDP-PXZ in toluene along the dihedral angle θ. The dihedral angle of TMBDP-PXZ at the equilibrium structure of the ground state was found to be $\theta = 80^\circ$, *i.e.*, BDP and PXZ are almost perpendicular due to the steric hindrance of the CH_3 groups, while that of BDP-PXZ was $\theta = 47^\circ$. In both systems, after the photo-irradiation θ will increase along the slope of the ^{1}CT state towards $\theta = 90^\circ$, where the ^{1}CT and ^{3}CT states are energetically very close due to the small exchange coupling for the perpendicular conformation. The shapes of PECs of ^{1}CT and ^{3}CT are similar for TMBDP-PXZ and BDP-PXZ systems, but that of the ^{3}BDP state is significantly different due to the presence and absence of the CH_3 group; the perpendicular structure ($\theta \simeq 90^\circ$) is the energy minimum in TMBDP-PXZ but is unstable in BDP-PXZ. In fact, in the perpendicular structure, the energy level of ^{3}BDP is lower by 0.4 eV than ^{1}CT and ^{3}CT states for TMBDP-PXZ, in contrast, it is very close in energy to ^{1}CT and ^{3}CT states for BDP-PXZ and as will be discussed ^{3}BDP and ^{3}CT are strongly mixed at around $\theta = 90^\circ$.

In the TMBDP-PXZ system, after the transition to either the ^{3}BDP or ^{3}CT state the wavepackets will immediately decay to the ^{3}BDP state, which lies at lower energy than the ^{3}CT state even in the solvent environment that minimizes the energy level of ^{3}CT as shown in Fig. 2b. In the BDP-PXZ system, the wavepackets that transit to the ^{3}CT state can stay on the ^{3}CT potential energy surface because ^{3}CT has lower energy than ^{3}BDP in the solvent reorganized for the ^{3}CT state, and the wavepacket that directly transits to the ^{3}BDP state from ^{1}CT state will stay in the ^{3}BDP state because it is lower in energy than ^{3}CT in the solvent reorganized for the ^{3}BDP state. This should be the reason why only the BDP-PXZ system exhibits the dual components in the TR-EPR spectra, while TMBDP-PXZ does not. Note that the state-specific effects, which can be evaluated by the corrected LR method[41,42] for example, were neglected in the calculations based on the LR-CPCM method. It may stabilize the excited states with the CT character and make it easier for ^{3}CT and ^{3}BDP to coexist. The detailed analysis for the difference in energetics caused by the CH_3 groups will be discussed in Section 3.4.

3.2 Spin polarization induced by intersystem crossing

To reveal the spin polarization axis in the molecular frame, which cannot be determined by the TR-EPR experiment for randomly oriented molecules, we computed the SOC matrix

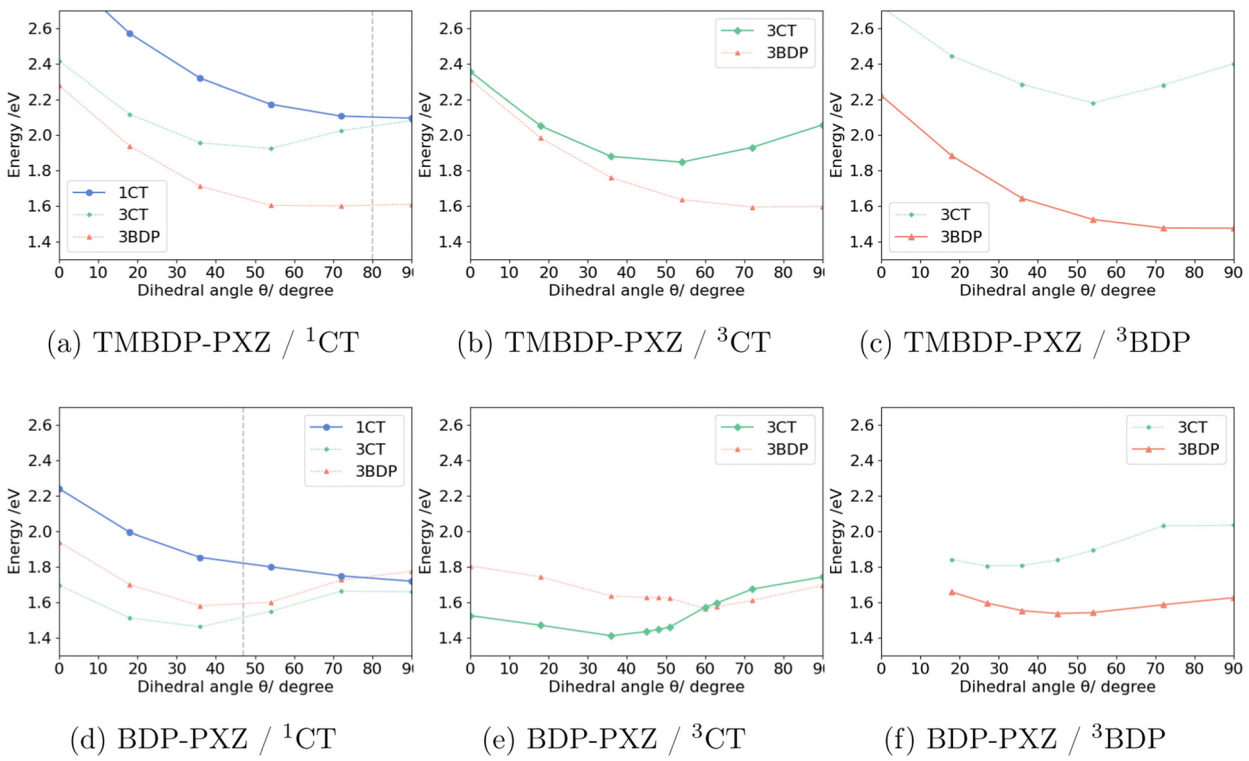

Fig. 2 Potential energy curves of ^{1}CT, ^{3}CT, and ^{3}BDP states along the dihedral angle between BDP and PXZ moieties, calculated with LC-BLYP/def2-TZVP under the solvent effect of toluene by LR-CPCM. The geometries were optimized for ^{1}CT: (a) and (d), ^{3}CT: (b) and (e), ^{3}BDP: (c) and (f) states of BDP-PXZ and TMBDP-PXZ with constraints for the dihedral angle θ between BDP and PXZ moieties. The target state is depicted with solid lines, while others with dotted lines; the former was calculated with an equilibrium solvent and the latter with a non-equilibrium solvent. The gray dashed lines in (a) and (d) indicate θ for the ground state stabilized structure.

elements between ^{1}CT and ^{3}CT ($\langle ^1\mathrm{CT}|H_{\mathrm{soc}}|^3\mathrm{CT}_\mu\rangle$) and ^{1}CT and ^{3}BDP ($\langle ^1\mathrm{CT}|H_{\mathrm{soc}}|^3\mathrm{BDP}_\mu\rangle$), where $\mu = x, y, z$ at the structures on the PECs of ^{1}CT in Fig. 2a and d. Table 1a and b show the SOC matrix elements of TMBDP-PXZ and BDP-PXZ, respectively, for each component $^3\mathrm{CT}_x$, $^3\mathrm{CT}_y$, and $^3\mathrm{CT}_z$ where x, y, and z correspond to the molecular axis of the BDP moiety shown in Fig. 3; the long axis is x, the short axis is y, and the out-of-plane axis is z. As shown in Table 1a, the SOC of $\langle ^1\mathrm{CT}|H_{\mathrm{soc}}|^3\mathrm{BDP}_\mu\rangle$ is x-polarized and significantly larger than that of $\langle ^1\mathrm{CT}|H_{\mathrm{soc}}|^3\mathrm{CT}_\mu\rangle$ at any dihedral angle θ.

Theoretically, the SOC is usually accounted by the change in the occupation of the atomic orbitals that have different angular momentum, *e.g.*, the change in the occupation of $2p_y$ and $2p_z$ orbitals, such as a lone pair orbital and π orbital, of an atom will contribute x-polarized SOC. As far as we know, it has never been explicitly analyzed, but the SOC in linked π-conjugated systems should originate from the transition between the in-plane (σ orbital) and out-of-plane (π orbital) associated with a charge transfer excitation. For example, Fig. 3 shows the canonical molecular orbitals that represent most of the transitions between ^{1}CT and ^{3}BDP at the $\theta = 90^\circ$ structure. The transition appears to involve the difference in occupations of $2p_x$ in the HOMO and $2p_z$ in HOMO−1 of the C7a and C8a atoms. It causes the change in the angular momentum about the x-axis and is considered to be the origin of the x-polarized SOC of ^{3}BDP shown in Table 1a and b. This is an explanation

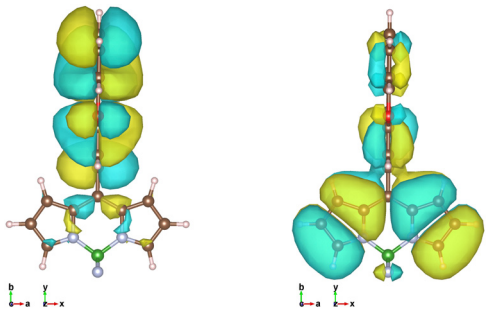

(a) HOMO (b) HOMO-1

Fig. 3 Surface plots of canonical MOs (isovalue = 0.008), calculated with LC-BLYP/def2-TZVP under the solvent effect of toluene by LR-CPCM, non-equilibrium condition.

for the mechanism of SOCT-ISC at the electronic level, *i.e.*, the reason why the SOC matrix elements between the charge transfer state and locally excited state in linked π-conjugated molecules are significant. The mechanism should be universal for other covalently linked π-conjugated systems, *e.g.*, the efficient reverse ISC of TADF. Note that an atom that is directly linked to the other aromatic moiety, the C8 atom in this case, usually has the largest contribution to this type of the generation of SOC because the in-plane $2p_x$ or $2p_y$ of the linked atom, which has the same symmetry as the π orbitals of the other aromatic moiety, can strongly mix with those, but the C8 atom happens to be located at the node of the π orbital of BDP in HOMO−1 and cannot contribute at least to the C_s ($\theta = 90^\circ$) structure.

For the same reasons, it is reasonable that the SOC matrix element $\langle ^1\mathrm{CT}|H_{\mathrm{soc}}|^3\mathrm{CT}_\mu\rangle$ for TMBDP-PXZ is weak because the transition between ^{1}CT and ^{3}CT does not involve the change in the electron configuration. It suggests that the direct transition from ^{1}CT to ^{3}BDP, which exhibits larger couplings than those with ^{3}CT by one or two order magnitudes, can occur through the minimum energy crossing point (MECP), which should be displaced along other degrees-of-freedom that are orthogonal to the minimum energy path of ^{1}CT shown in Fig. 2a. In fact, we found that the MECP is located at $\theta = 87^\circ$ with less than 7 kcal mol^{-1} above the energy minimum of ^{1}CT state (see the ESI†), so the direct transition to ^{3}BDP should be quite feasible. Note that the energy gap between ^{3}BDP and ^{3}CT should be small at around the MECP, and two triplet states can be strongly mixed and an ISC transition to ^{3}CT could be possible by borrowing the x-polarized SOC of ^{3}BDP, although it should soon decay to the lower energy state ^{3}BDP anyway without changing the polarization in the molecular frame conserving the angular momentum. For BDP-PXZ, in which the mixture of two components observed in the TR-EPR spectra,[27] not only ^{3}BDP but also ^{3}CT should be generated although the transition from ^{1}CT to ^{3}CT is considered to be inefficient due to the weak coupling character as explained above. As can be seen in Table 1b, however, the SOC matrix element between ^{1}CT and ^{3}CT is large enough ($\sim$0.5 cm^{-1}) at around $\theta = 90^\circ$ structure.

Table 1 The SOC matrix elements $\langle ^1\mathrm{CT}|H_{\mathrm{soc}}|^3\mathrm{CT}_\mu\rangle$ and $\langle ^1\mathrm{CT}|H_{\mathrm{soc}}|^3\mathrm{BDP}_\mu\rangle$ for the TMBDP-PXZ and the BDP-PXZ, along with ΔE indicating the energy gaps (^{1}CT–^{3}CT) and (^{1}CT–^{3}BDP), calculated with LC-BLYP/def2-TZVP under the solvent effect of toluene by LR-CPCM, non-equilibrium condition

θ	0°	18°	36°	54°	72°	90°
(a) TMBDP-PXZ						
$\lvert\langle ^1\mathrm{CT}\lvert H_{\mathrm{soc}}\rvert ^3\mathrm{CT}_\mu\rangle\rvert$/cm^{-1}						
x	0.11	0.09	0.05	0.01	0.01	0.01
y	0.03	0.07	0.11	0.14	0.14	0.02
z	0.00	0.01	0.00	0.01	0.02	0.01
ΔE/eV						
	0.52	0.45	0.36	0.25	0.08	0.01
$\lvert\langle ^1\mathrm{CT}\lvert H_{\mathrm{soc}}\rvert ^3\mathrm{BDP}_\mu\rangle\rvert$/cm^{-1}						
x	0.29	0.39	0.47	0.56	0.66	0.71
y	0.13	0.11	0.08	0.03	0.03	0.01
z	0.02	0.01	0.03	0.03	0.04	0.01
ΔE/eV						
	0.66	0.63	0.61	0.57	0.51	0.49
(b) BDP-PXZ						
$\lvert\langle ^1\mathrm{CT}\lvert H_{\mathrm{soc}}\rvert ^3\mathrm{CT}_\mu\rangle\rvert$/cm^{-1}						
x	0.00	0.03	0.03	0.11	0.44	0.48
y	0.07	0.13	0.15	0.15	0.06	0.00
z	0.01	0.01	0.00	0.02	0.01	0.00
ΔE/eV						
	0.54	0.48	0.39	0.25	0.09	0.06
$\lvert\langle ^1\mathrm{CT}\lvert H_{\mathrm{soc}}\rvert ^3\mathrm{BDP}_\mu\rangle\rvert$/cm^{-1}						
x	0.22	0.33	0.40	0.52	0.52	0.56
y	0.04	0.02	0.01	0.03	0.05	0.00
z	0.02	0.02	0.00	0.03	0.01	0.00
ΔE/eV						
	0.30	0.29	0.27	0.20	0.02	−0.06

This should be explained by the state mixing of ^{3}CT and ^{3}BDP; those are very close in energy at around θ = 90° structure (Fig. 2d). Indeed, it was found that the electron configurations of the ^{3}CT state obtained by TDDFT consist of 57.6% HOMO of PXZ → LUMO of BDP (^{3}CT configuration) and 38.7% HOMO of BDP → LUMO of BDP (^{3}BDP configuration). The latter configuration should contribute to the large *x*-polarized SOC of ^{3}CT in BDP-PXZ.

3.3 Prediction of the ZFS *D*-tensor in the molecular frame

The ZFS *D*-tensor in the molecular frame was calculated at the level of DMRG-CASSCF theory, in which the active space consists of the full valence π orbitals CAS(28e, 25o), and diagonalized to assign the magnetic axis in the molecular frame; the method is described in detail in ref. 29. Table 2 summarizes ZFS of the spin sublevels of ^{3}BDP and ^{3}CT for BDP-PXZ, and the polarization axis with the correspondence between the molecular axes *x*, *y*, and *z* and magnetic axes *x*′, *y*′, and *z*′ for ^{3}BDP and *x*″, *y*″, *z*″ for ^{3}CT. The ZFS parameters, *D* and *E* values, were predicted to be −79.44 mT and 6.87 mT for ^{3}BDP at the ^{3}BDP energy minimum structure and −44.24 mT and 17.75 mT for ^{3}CT at the ^{3}CT energy minimum structure, respectively. The predicted *D* values are in good agreement with the values determined by the TR-EPR spectra in ref. 27. There are discrepancies in the trend between the theoretical and the experimental *E* values, of which the absolute value is often small and sensitive to the change in the *D*-tensor.[29] In addition, the magnetic axis in the molecular frame was determined by diagonalizing the *D* tensor, and it was found that the *x*-axis, which is the axis of the electron polarization induced by the spin-selective ISC from ^{1}CT (see Section 3.2), corresponds to the *z*′ and *y*″ for ^{3}BDP and ^{3}CT, respectively. It is also consistent with the TR-EPR experiments, which strongly support the proposed molecular mechanism in Section 3.1.

3.4 Insights into the molecular mechanism

As proposed using the theoretical calculations and confirmed by the consistency between the calculations and the experiments of the TR-EPR measurement, the transitions from ^{1}CT to ^{3}CT and ^{3}BDP should occur at around the θ = 90° structure, hence the steric hindrance by CH_3 groups of TMBDP-PXZ is not critical to the mechanism, rather the electron donor character of the groups, which should affect the energy levels of the HOMO and LUMO of the BDP moiety, seems to be more important for the mechanism.

Table 2 ZFS of the triplet sublevels of ^{3}BDP and ^{3}CT, and the correspondence between the molecular axes *x*, *y*, *z* (Fig. 3) and magnetic axes *x*′, *y*′, *z*′ for ^{3}BDP and *x*″, *y*″, *z*″ for ^{3}CT. The values are calculated with (28e, 25o) DMRG-CASSCF

		D/mT	*E*/mT	Polarization
Calc				
	^{3}BDP	−79.44	6.87	*x* (= *z*′)
	^{3}CT	−44.24	17.75	*x* (= *y*″)
Expt[a]				
	^{3}BDP	−82.1	19.1	*z*′
	^{3}CT	−37.5	8.2	*y*″

[a] Ref. 27.

Table 3 HOMO, LUMO, and T_1 excitation energies in eV of the BDP monomer, calculated with LC-BLYP/def2-TZVP under the solvent effect of toluene by LR-CPCM, non-equilibrium condition

	HOMO	LUMO	T_1
BDP	−7.44	−2.00	1.71
TMBDP	−6.76	−1.54	1.56

Regarding this point, the TD-DFT calculation for the BDP monomer was performed. As summarized in Table 3, when CH_3 groups were added, both the HOMO and LUMO energies of the BDP monomer increase by 0.67 eV and 0.45 eV, respectively, and the excitation energy of ^{3}BDP slightly decreases by 0.15 eV. It should have more impacts on ^{3}CT because only the LUMO of BDP, which accepts the electrons from the HOMO of the donor PXZ that should not be altered by the substitution of CH_3 to the BDP moiety, is involved in the charge transfer. Thus only the ^{3}BDP is observed for TMBDP-PXZ, whereas the ^{3}CT is observed together with ^{3}BDP for BDP-PXZ in the TR-EPR measurements.

To investigate the impact of the electron-withdrawing/donating groups on the BDP moiety, the potential energy curves were constructed for three other BDP-PXZ derivatives with different substituent groups X (X = Me, NO_2, and NH_2) on C3 and C5 atoms in BDP, where the groups bring an insignificant steric effect to the PXZ moiety (Fig. 4). The curves have similar shapes throughout θ, the dihedral angles between BDP and PXZ moieties as reaction coordinates; however quite different in energy levels of ^{3}CT and ^{3}BDP (see the ESI†).

Moreover, with a series of various substituent groups (X = F, Cl, NH_2, OMe, Me, H, CF_3, Ac, CHO, CN, and NO_2) on the C3 and C5 atoms of BDP moiety, the scatter plots between the Hammett substituent constants and the energy levels of ^{1}CT, ^{3}CT, and ^{3}BDP states were obtained, as the positive substituent constants correspond to electron-withdrawing groups while the negatives to electron-donating groups.[43] The energy levels are calculated using the optimized structures under the constraints for the dihedral angle θ = 90° for clarity. As shown in Fig. 5, there were certain correlations between the substituent

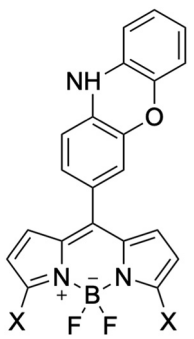

Fig. 4 Chemical structures of BDP-PXZ derivatives with substituent groups X, as X = Me, NO_2, and NH_2 in potential energy curve analysis, and X = F, Cl, NH_2, OMe, Me, H, CF_3, Ac, CHO, CN, and NO_2 in Hammett substituent constant analysis.

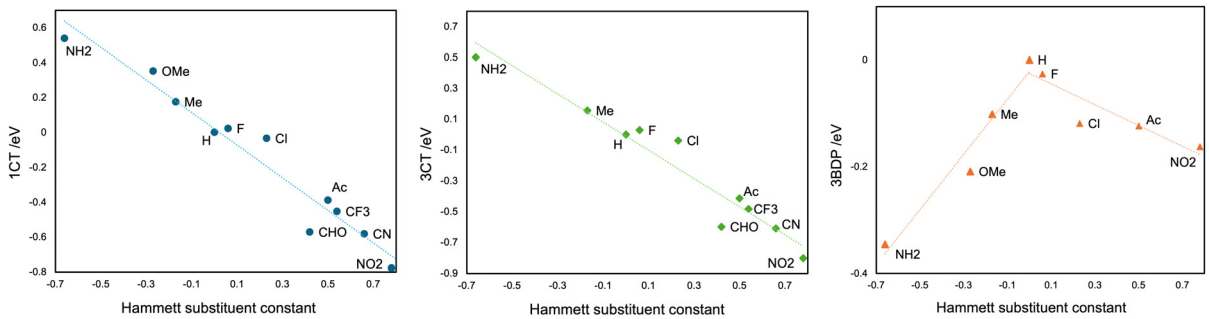

Fig. 5 The scatter plot between the Hammett substituent constants and the energy levels of ^{1}CT, ^{3}CT, and ^{3}BDP states for BDP-PXZ derivatives with a series of different substituent groups, calculated with LC-BLYP/def2-TZVP under the solvent effect of toluene by LR-CPCM, equilibrium condition.

constant and ^{1}CT and ^{3}CT energy levels; the correlation coefficient was −0.973 for ^{1}CT, and −0.967 for ^{3}CT, respectively. This result makes it clear that the electron-donating groups on the C3 and C5 atoms of BDP raise the energy level of ^{1,3}CT states, as the BDP-LUMO level gets higher, and *vice versa*. On the other hand, the ^{3}BDP level is the highest when X = H, and it gets lower for both electron-donating and withdrawing groups. It is natural, considering that the ^{3}BDP state involves not only BDP-LUMO but also BDP-HOMO. In this way, it was reasonably elucidated that the electron donor character of the groups, which should affect the energy levels of the HOMO and the LUMO of the BDP moiety, is more important for the formation mechanism of ^{3}CT and ^{3}BDP transient species, rather than their steric hindrance. The different dependencies of the CT and LE excited states on the substituent effects should be useful for designing molecules that meet the necessary condition of an efficient SOCT that the energy levels of the singlet and triplet charge transfer states lie between those of the singlet and triplet local excited states.

4 Summary

We revealed the details of the triplet formation process of BDP-PXZ and TMBDP-PXZ *via* the SOCT-ISC; the reason why the two different triplet transient species were experimentally observed for BDP-PXZ, and only one species for TMBDP-PXZ, even though the structures differ only by the substitution of the methyl groups. As shown in the analysis of the potential energy curves along the dihedral angles between BDP and PXZ moieties as the reaction coordinates, in both molecules the transition from ^{1}CT to either the ^{3}BDP or ^{3}CT state occurs at about the orthogonal conformation, where the ^{1}CT and ^{3}CT states are close in energy.

In BDP-PXZ, it was found that the wavepacket that transits to the ^{3}CT and ^{3}BDP states can remain on their adiabatic potential energy surface because both states are the lowest triplet states in their solvent environment. In TMBDP-PXZ, on the other hand, the ^{3}BDP state is more stable than the ^{3}CT state even in the solvent environment that is optimized for the ^{3}CT state, and only the ^{3}BDP state will be observed regardless of which triplet excited state surfaces the wavepacket has at first transited to. The key to this difference is therefore not the steric hindrance, but the electron donating effect of the CH_3 groups on the BDP moiety, which increases the energy levels of the BDP's HOMO and LUMO to elevate the ^{3}CT.

Utilizing the correlation analysis between the energy levels of the excited states and Hammett substituent constants, it was reasonably elucidated that the electron-donating/withdrawing substituent groups on the BDP moiety are strongly correlated with ^{1,3}CT states; and with ^{3}BDP, have an analogous trend with the CT state for electron-withdrawing groups, while the opposite trend for electron-donating ones. It should be universal for the ^{3}CT and ^{3}BDP states of dyad systems and can be exploited to control the formation process of the triplet state by the SOCT-ISC.

Furthermore, with the calculation of the spin–orbit coupling matrix element between ^{1}CT and each triplet state, it was shown that the triplet states generated by the SOCT-ISC should be spin polarized to the component of the BDP's long axis (^3CT_x and $^3BDP_x$). This result, together with the prediction of the ZFS tensor in the molecular frame, is quite consistent with the TR-EPR spectral results, which strongly supports the SOCT-ISC mechanism we propose. Our theoretical study has reasonably discovered the fundamental mechanisms of the triplet formation of BDP-PXZ systems and the effect of the molecular structures. These insights would be a compass to molecular design of metal-free triplet photosensitizers.

Author contributions

Y. K. conceived the project, M. K. carried out the calculations and analyzed the computational results, K. M. and Y. K. partly contributed to the calculations, and M. K. and Y. K. participated in the composition and revision of the manuscript.

Data availability

The data supporting this study's findings are available from the corresponding authors upon reasonable request.

Conflicts of interest

There are no conflicts to declare.

Acknowledgements

This work was partly supported by the JST-FOREST Program (JPMJFR221R), JST-CREST Program (JPMJCR23I6), MEXT Q-LEAP Program (JPMXS0120319794), JSPS KAKENHI (JP23K 26614), and Tokyo Ohka Foundation for The Promotion of Science and Technology. The computation was partly performed at the Research Center for Computational Science, Okazaki, Japan (Project: 24-IMS-C028).

References

1 R. Pérez-Ruiz, Photon Upconversion Systems Based on Triplet–Triplet Annihilation as Photosensitizers for Chemical Transformations, *Top. Curr. Chem.*, 2022, **380**, 23.
2 N. Yanai and N. Kimizuka, New Triplet Sensitization Routes for Photon Upconversion: Thermally Activated Delayed Fluorescence Molecules, Inorganic Nanocrystals, and Singlet-to-Triplet Absorption, *Acc. Chem. Res.*, 2017, **50**, 2487–2495.
3 T. N. Singh-Rachford and F. N. Castellano, Photon Upconversion Based on Sensitized Triplet–Triplet Annihilation, *Coord. Chem. Rev.*, 2010, **254**, 2560–2573.
4 J. Zhou, Q. Liu, W. Feng, Y. Sun and F. Li, Upconversion Luminescent Materials: Advances and Applications, *Chem. Rev.*, 2015, **115**, 395–465.
5 M. Zhong and Y. Sun, Recent Advancements in the Molecular Design of Deep-Red to near-Infrared Light-Absorbing Photocatalysts, *Chem Catal.*, 2024, 100973.
6 V.-N. Nguyen, Y. Yan, J. Zhao and J. Yoon, Heavy-Atom-Free Photosensitizers: From Molecular Design to Applications in the Photodynamic Therapy of Cancer, *Acc. Chem. Res.*, 2021, **54**, 207–220.
7 X. Zhang, Z. Wang, Y. Hou, Y. Yan, J. Zhao and B. Dick, Recent Development of Heavy-Atom-Free Triplet Photosensitizers: Molecular Structure Design, Photophysics and Application, *J. Mater. Chem. C*, 2021, **9**, 11944–11973.
8 M. A. Filatov, Heavy-Atom-Free BODIPY Photosensitizers with Intersystem Crossing Mediated by Intramolecular Photoinduced Electron Transfer, *Org. Biomol. Chem.*, 2020, **18**, 10–27.
9 J. Großkopf, T. Kratz, T. Rigotti and T. Bach, Enantioselective Photochemical Reactions Enabled by Triplet Energy Transfer, *Chem. Rev.*, 2022, **122**, 1626–1653.
10 C.-C. Ko and V. W.-W. Yam, Coordination Compounds with Photochromic Ligands: Ready Tunability and Visible Light-Sensitized Photochromism, *Acc. Chem. Res.*, 2018, **51**, 149–159.
11 T. Hamachi and N. Yanai, Recent Developments in Materials and Applications of Triplet Dynamic Nuclear Polarization, *Prog. Nucl. Magn. Reson. Spectrosc.*, 2024, **142–143**, 55–68.
12 K. Nishimura, H. Kouno, Y. Kawashima, K. Orihashi, S. Fujiwara, K. Tateishi, T. Uesaka, N. Kimizuka and N. Yanai, Materials Chemistry of Triplet Dynamic Nuclear Polarization, *Chem. Commun.*, 2020, **56**, 7217–7232.
13 A. Kagawa, M. Negoro, K. Takeda and M. Kitagawa, Magnetic-Field Cycling Instrumentation for Dynamic Nuclear Polarization-Nuclear Magnetic Resonance Using Photoexcited Triplets, *Rev. Sci. Instrum.*, 2009, **80**, 044705.
14 K. Takeda, K. Takegoshi and T. Terao, Dynamic Nuclear Polarization by Electron Spins in the Photoexcited Triplet State: I. Attainment of Proton Polarization of 0.7 at 105 K in Naphthalene, *J. Phys. Soc. Jpn.*, 2004, **73**, 2313–2318.
15 Z. E. X. Dance, S. M. Mickley, T. M. Wilson, A. B. Ricks, A. M. Scott, M. A. Ratner and M. R. Wasielewski, Intersystem Crossing Mediated by Photoinduced Intramolecular Charge Transfer: Julolidine-Anthracene Molecules with Perpendicular π Systems, *J. Phys. Chem. A*, 2008, **112**, 4194–4201.
16 C. V. Suneesh and K. R. Gopidas, Long-Lived Photoinduced Charge Separation Due to the Inverted Region Effect in 1,6-Bis(Phenylethynyl)pyrene-Phenothiazine Dyad, *J. Phys. Chem. C*, 2010, **114**, 18725–18734.
17 G. Ulrich, R. Ziessel and A. Harriman, The Chemistry of Fluorescent Bodipy Dyes: Versatility Unsurpassed, *Angew. Chem., Int. Ed.*, 2008, **47**, 1184–1201.
18 N. Boens, V. Leen and W. Dehaen, Fluorescent Indicators Based on BODIPY, *Chem. Soc. Rev.*, 2012, **41**, 1130–1172.
19 M. A. Filatov, S. Karuthedath, P. M. Polestshuk, H. Savoie, K. J. Flanagan, C. Sy, E. Sitte, M. Telitchko, F. Laquai, R. W. Boyle and M. O. Senge, Generation of Triplet Excited States *via* Photoinduced Electron Transfer in Meso -Anthra-BODIPY: Fluorogenic Response toward Singlet Oxygen in Solution and in Vitro, *J. Am. Chem. Soc.*, 2017, **139**, 6282–6285.
20 K. Suzuki and H. Kaji, Torsion Angle Analysis of a Thermally Activated Delayed Fluorescence Emitter in an Amorphous State Using Dynamic Nuclear Polarization Enhanced Solid-State NMR, *J. Am. Chem. Soc.*, 2023, jacs.3c05204.
21 S. Sasaki, G. P. C. Drummen and G.-I. Konishi, Recent Advances in Twisted Intramolecular Charge Transfer (TICT) Fluorescence and Related Phenomena in Materials Chemistry, *J. Mater. Chem. C*, 2016, **4**, 2731–2743.
22 Z. R. Grabowski, K. Rotkiewicz and W. Rettig, Structural Changes Accompanying Intramolecular Electron Transfer: Focus on Twisted Intramolecular Charge-Transfer States and Structures, *Chem. Rev.*, 2003, **103**, 3899–4032.
23 H. Uoyama, K. Goushi, K. Shizu, H. Nomura and C. Adachi, Highly Efficient Organic Light-Emitting Diodes from Delayed Fluorescence, *Nature*, 2012, **492**, 234–238.
24 F. B. Dias, T. J. Penfold and A. P. Monkman, Photophysics of Thermally Activated Delayed Fluorescence Molecules, *Methods Appl. Fluoresc.*, 2017, **5**, 012001.
25 Y. Tao, K. Yuan, T. Chen, P. Xu, H. Li, R. Chen, C. Zheng, L. Zhang and W. Huang, Thermally Activated Delayed Fluorescence Materials Towards the Breakthrough of Organoelectronics, *Adv. Mater.*, 2014, **26**, 7931–7958.
26 Z. Yang, Z. Mao, Z. Xie, Y. Zhang, S. Liu, J. Zhao, J. Xu, Z. Chi and M. P. Aldred, Recent Advances in Organic Thermally Activated Delayed Fluorescence Materials, *Chem. Soc. Rev.*, 2017, **46**, 915–1016.
27 Y. Dong, A. A. Sukhanov, J. Zhao, A. Elmali, X. Li, B. Dick, A. Karatay and V. K. Voronkova, Spin–Orbit Charge-Transfer

Intersystem Crossing (SOCT-ISC) in Bodipy-Phenoxazine Dyads: Effect of Chromophore Orientation and Conformation Restriction on the Photophysical Properties, *J. Phys. Chem. C*, 2019, **123**, 22793–22811.

28 K. Sakamoto, T. Hamachi, K. Miyokawa, K. Tateishi, T. Uesaka, Y. Kurashige and N. Yanai, Polarizing agents beyond pentacene for efficient triplet dynamic nuclear polarization in glass matrices, *Proc. Natl. Acad. Sci. U. S. A.*, 2023, **120**, e2307926120.

29 K. Miyokawa and Y. Kurashige, Zero-Field Splitting Tensor of the Triplet Excited States of Aromatic Molecules: A Valence Full-π Complete Active Space Self-Consistent Field Study, *J. Phys. Chem. A*, 2024, **128**, 2349–2356.

30 F. Weigend and R. Ahlrichs, Balanced Basis Sets of Split Valence, Triple Zeta Valence and Quadruple Zeta Valence Quality for H to Rn: Design and Assessment of Accuracy, *Phys. Chem. Chem. Phys.*, 2005, **7**, 3297.

31 F. Weigend, Accurate Coulomb-fitting Basis Sets for H to Rn, *Phys. Chem. Chem. Phys.*, 2006, **8**, 1057.

32 A. Hellweg, C. Hättig, S. Höfener and W. Klopper, Optimized Accurate Auxiliary Basis Sets for RI-MP2 and RI-CC2 Calculations for the Atoms Rb to Rn, *Theor. Chem. Acc.*, 2007, **117**, 587–597.

33 Y. Tawada, T. Tsuneda, S. Yanagisawa, T. Yanai and K. Hirao, A Long-Range-Corrected Time-Dependent Density Functional Theory, *J. Chem. Phys.*, 2004, **120**, 8425–8433.

34 V. Barone and M. Cossi, Quantum Calculation of Molecular Energies and Energy Gradients in Solution by a Conductor Solvent Model, *J. Phys. Chem. A*, 1998, **102**, 1995–2001.

35 F. Neese, Software Update: The ORCA Program System—Version 5.0, *Wiley Interdiscip. Rev.: Comput. Mol. Sci.*, 2022, **12**, e1606.

36 D. Zgid and M. Nooijen, The Density Matrix Renormalization Group Self-Consistent Field Method: Orbital Optimization with the Density Matrix Renormalization Group Method in the Active Space, *J. Chem. Phys.*, 2008, **128**, 144116.

37 D. Ghosh, J. Hachmann, T. Yanai and G. K.-L. Chan, Orbital Optimization in the Density Matrix Renormalization Group, with Applications to Polyenes and \beta-Carotene, *J. Chem. Phys.*, 2008, **128**, 144117.

38 T. Yanai, Y. Kurashige, D. Ghosh and G. K.-L. Chan, Accelerating Convergence in Iterative Solution for Large-Scale Complete Active Space Self-Consistent-Field Calculations, *Int. J. Quantum Chem.*, 2009, **109**, 2178–2190.

39 D. Ganyushin, N. Gilka, P. R. Taylor, C. M. Marian and F. Neese, The Resolution ofthe Identity Approximation for Calculations of Spin-Spin Contribution to Zero-Field Splitting Parameters, *J. Chem. Phys.*, 2010, **132**, 144111.

40 Q. Sun, T. C. Berkelbach, N. S. Blunt, G. H. Booth, S. Guo, Z. Li, J. Liu, J. D. McClain, E. R. Sayfutyarova, S. Sharma, S. Wouters and G. K.-L. Chan, P y SCF: The Python-based Simulations of Chemistry Framework, *Wiley Interdiscip. Rev.: Comput. Mol. Sci.*, 2018, 8.

41 M. Caricato, B. Mennucci, J. Tomasi, F. Ingrosso, R. Cammi, S. Corni and G. Scalmani, Formation and Relaxation of Excited States in Solution: A New Time Dependent Polarizable Continuum Model Based on Time Dependent Density Functional Theory, *J. Chem. Phys.*, 2006, **124**, 124520.

42 S. Chibani, A. D. Laurent, B. Le Guennic and D. Jacquemin, Improving the Accuracy of Excited-State Simulations of BODIPY and Aza-BODIPY Dyes with a Joint SOSCIS(D) and TD-DFT Approach, *J. Chem. Theory Comput.*, 2014, **10**, 4574–4582.

43 C. Hansch, A. Leo and R. W. Taft, A Survey of Hammett Substituent Constants and Resonance and Field Parameters, *Chem. Rev.*, 1991, **91**, 165–195.

